7. Zaritsky, D. & Lo, K. Y. *Astrophys. J.* **303,** 66–75 (1986).
8. Ishizuki, S. *et al. Astrophys. J.* **355,** 436–441 (1990).
9. Regan, M. W. & Vogel, S. N. *Astrophys. J.* **452,** L21–L24 (1995).
10. Rogstad, D. H., Shostak, G. S. & Rots, A. H. *Astron. Astrophys.* **22,** 111–119 (1973).
11. Tacconi, L. J. & Young, J. S. *Astrophys. J.* **308,** 600–610 (1986).
12. Carignan, C., Charbonneau, P., Boulanger, F. & Viallefond, F. *Astron. Astrophys.* **234,** 43–52 (1990).
13. Binney, J. & Tremaine, S. *Galactic Dynamics* (Princeton Univ. Press, 1987).
14. Lin, C. C. & Shu, F. H. *Astrophys. J.* **140,** 646–655 (1964).
15. Lin, C. C. & Shu, F. H. *Proc. Natl Acad. Sci. USA* **55,** 229–234 (1966).
16. Athanassoula, E. *Phys. Rep.* **114,** 319–403 (1984).
17. Roberts, W. W. Jr & Yuan, C. *Astrophys. J.* **161,** 887–902 (1970).
18. Krause, M. in *The Cosmic Dynamo* (eds Krause, F., Rädler, K. H. & Rüdiger, G.) 305–310 (Int. Astron. Union Symp. No. 157, Kluwer Academic, Dordrecht, 1993).
19. Neininger, N., Beck, R., Sukumar, S. & Allen, R. J. *Astron. Astrophys.* **274,** 687–698 (1993).
20. Goldreich, P. & Lynden-Bell, D. *Mon. Not. R. Astron. Soc.* **130,** 125–158 (1965).
21. Bertin, G. & Lin, C. C. *Spiral Structure in Galaxies: A Density Wave Theory* (MIT Press, 1996).
22. Bardeen, J. M. in *Dynamics of Stellar Systems* (ed. Hayli, A.) 297–320 (Int. Astron. Union, Symp. No. 69, Reidel, Dordrecht, 1975).
23. Shu, F. H. *Astrophys. J.* **160,** 99–112 (1970).
24. Toomre, A. *Annu. Rev. Astron. Astrophys.* **15,** 437–478 (1977).
25. Chandrasekhar, S. & Fermi, E. *Astrophys. J.* **118,** 116–141 (1953).
26. Lynden-Bell, D. *Observatory* **86,** 57–60 (1966).
27. Lou, Y. Q. *Mon. Not. R. Astron. Soc.* **279,** L67–L70 (1996).
28. Miller, R. H., Prendergast, K. H. & Quirk, W. J. *Astrophys. J.* **161,** 903–916 (1970).
29. Ostriker, J. P. & Peebles, P. J. E. *Astrophys. J.* **186,** 467–480 (1973).
30. Vandervoort, P. *Astrophys. J.* **162,** 453–462 (1970).
31. Parker, E. N. *Astrophys. J.* **401,** 137–145 (1992).
32. Chakrabarti, S. K., Vainstein, S. I. & Rosner, R. *Nature* **368,** 434–436 (1994).
33. Mestel, L. & Subramanian, K. *Mon. Not. R. Astron. Soc.* **248,** 677–687 (1991).
34. Otmianowska-Mazur, K. & Chiba, M. *Astron. Astrophys.* **301,** 41–54 (1995).

ACKNOWLEDGEMENTS. This work was supported by the US NSF and NASA.

CORRESPONDENCE should be addressed to Y.-Q.L. (e-mail: lou@oddjob.uchicago.edu).

Fluorescence intermittency in single cadmium selenide nanocrystals

M. Nirmal*†, B. O. Dabbousi*, M. G. Bawendi*, J. J. Macklin†‡, J. K. Trautman†‡, T. D. Harris†‡, & L. E. Brus†‡

* Massachusetts Institute of Technology, Dept of Chemistry, 77 Massachusetts Avenue, Cambridge, Massachusetts 02139, USA
‡ Bell Laboratories, Lucent Technologies, 600 Mountain Avenue, Murray Hill, New Jersey 07974, USA

SEMICONDUCTOR nanocrystals offer the opportunity to study the evolution of bulk materials properties as the size of a system increases from the molecular scale[1,2]. In addition, their strongly size-dependent optical properties render them attractive candidates as tunable light absorbers and emitters in optoelectronic devices such as light-emitting diodes[3,4] and quantum-dot lasers[5,6], and as optical probes of biological systems[7]. Here we show that light emission from single fluorescing nanocrystals of cadmium selenide under continuous excitation turns on and off intermittently with a characteristic timescale of about 0.5 seconds. This intermittency is not apparent from ensemble measurements on many nanocrystals. The dependence on excitation intensity and the change in on/off times when a passivating, high-bandgap shell of zinc sulphide encapsulates the nanocrystal[8,9] suggests that the abrupt turning off of luminescence is caused by photoionization of the nanocrystal. Thus spectroscopic measurements on single nanocrystals can reveal hitherto unknown aspects of their photophysics.

In Fig. 1*a* we show a fluorescence image of single 21-Å-radius CdSe nanocrystals, embedded in a thin polyvinylbutyral film, at room temperature. The streaks in the image are a consequence of raster scanning the sample across a diffraction-limited laser spot, and arise due to the discrete turning on and off of the nanocrystal fluorescence signal while acquiring the image (~2 min). A fluorescence intensity versus time trace for a single nanocrystal under continuous wave excitation is shown in Fig. 1*b*.

To determine whether this on/off phenomenon is light-induced or occurs spontaneously we investigated the intensity dependence of the on/off times. If the ons/offs were due to spontaneous transformations between an emitting and a 'dark' configuration, the on/off periods would be independent of excitation intensity[10]. On the other hand, for a light-induced process where the 'dark' state is fed via a radiationless transition from the optically excited state, the 'on' times should decrease with increasing excitation intensity whereas the 'off' times would be determined by the spontaneous lifetime of the 'dark' state[11]. Fluorescence intensity versus time traces at two excitation intensities (Fig. 2*a*) indicate that the average on time is inversely proportional to the excitation intensity while the average off time is intensity independent, suggesting a light-induced process.

This on/off behaviour is consistent with a mechanism based on Auger ionization. In nanocrystals with two or more electron–hole pairs, the energy released from the annihilation of a pair may be transferred to the remaining carriers, one of which is preferentially ejected into the surrounding matrix depending on the conduction (valence) band offset at the nanocrystal interface and the electron (hole) confinement energy within the nanocrystal. In the resulting ionized nanocrystal, the Auger interaction, which is mediated by the Coulomb repulsive potential between carriers, is strongly enhanced owing to the diminished screening relative to neutral nanocrystals. Subsequent photogenerated electron–hole pairs thus recombine primarily non-radiatively, transferring their energy to the resident carrier. This mechanism accounts for the decrease in the quantum efficiency of similar CdS nanocrystals embedded in glass on laser irradiation (photodarkening)[12]. Photodarkened particles exhibit significantly shorter

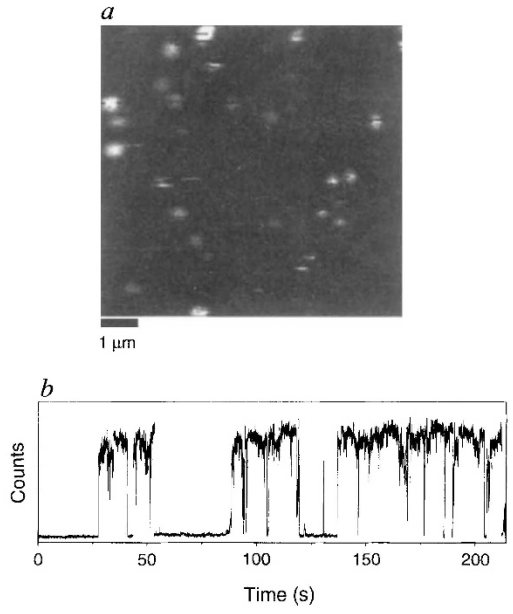

FIG. 1 *a*, Image of a random field of single ~21-Å-radius CdSe nanocrystals (each with ~4 monolayers of ZnS on its surface) acquired by raster scanning the sample across a diffraction-limited laser spot (wavelength 532 nm, full-width at half-maximum ~0.38 μm) and collecting the red-shifted fluorescence onto an avalanche photodiode in an epi-illumination confocal geometry[19]. This 160 × 160 pixel image (1 pixel = 5 ms) represents an 8 × 8 μm field of view. Sample preparation involves spin-coating one drop of a ~5 nM solution of nanocrystals in a 0.5% polyvinylbutyral/toluene mixture onto a quartz cover slip. *b*, Fluorescence intensity versus time trace of a single ~21-Å-radius CdSe nanocrystal, from the same sample used in *a*, recorded using a multichannel scaler with a 40-ms sampling interval and an excitation intensity of ~0.52 kW cm^{-2}.

† Present addresses: Department of Chemistry, Columbia University, New York, New York 10027, USA (M.N., L.E.B.); seQ Ltd, Princeton, New Jersey 08540-6449, USA (J.J.M., J.K.T., T.D.H.)

emission lifetimes and lower quantum yield relative to neutral nanocrystals[13]. The luminescence is then restored when the ejected carrier returns to neutralize the particle. At low flux (about three orders of magnitude lower than in our study) the Auger ionization rate was observed to scale as the square of the excitation intensity[12]. We observe that the average on period, which is determined by the ionization rate, scales linearly with intensity (Fig. 2*a*). Furthermore, mode-locked pulsed laser excitation at the same average power but with over two orders of magnitude higher probability of generating two electron–hole pairs, yielded similar on times as were found with continuous-wave excitation. This suggests a two-step ionization mechanism. The first step involves trapping of one of the carriers onto the nanocrystal surface followed by photoionization within the trap state lifetime (~5 μs). At low flux both processes should scale linearly with excitation intensity (I), the quantum yield of the ionization step being $[(I\sigma_p)/(h\nu)]/\{[(I\sigma_p)/(h\nu)] + \gamma_t\}$, where σ_p is the photoionization cross-section and γ_t is the relaxation rate from the intermediate trap state. Saturation of either step would lead to a net linear dependence. For instance, at an excitation rate of ~1 MHz as in our study, a trap lifetime of ~5 μs and assuming an ionization yield of ~10–100%, the second step would approach saturation resulting in an effective three-level system with near-linear intensity dependence.

Based on this model the on/off times, determined by the photoionization/neutralization rates respectively, should be sensitive to changes at the nanocrystal–matrix interface. The nanocrystals as initially synthesized ('bare') have organic capping groups which passivate ~1/2 of all the surface atoms[14,15]. These particles can instead by overcoated with a shell of ZnS, a higher-bandgap material[8,9], with the organic capping groups on the ZnS surface. In Fig. 2*b*, the fluorescence intensity versus time trace of a 'bare' particle is compared at the same excitation intensity with that of an overcoated one (with ~7 monolayers of ZnS). ZnS has a bandgap ~2 eV higher than that of CdSe and so should serve as an effective barrier to ionization/neutralization and passivate potential surface trap sites. This is apparent in the dramatic increase in both the average on/off times for the ZnS overcoated nanocrystal relative to the 'bare' particle. To confirm this, we probed on/off times at the same excitation intensity as a function of shell thickness for CdSe nanocrystals with 0, ~0.25, ~2 and ~7 monolayers of ZnS. Strongly non-exponential histograms of on/off times for the four samples are shown in Fig. 3*a* and *b*. Each histogram represents on/off statistics for 18 nanocrystals. The

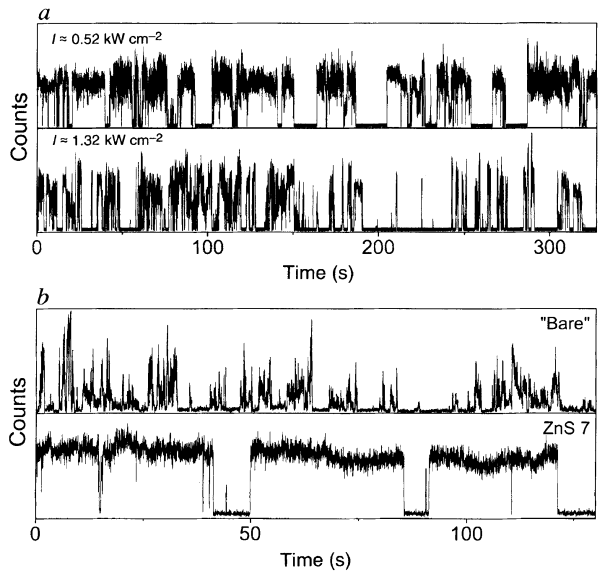

FIG. 2 *a*, Comparison of fluorescence-intensity versus time traces at excitation intensities (I) of ~0.52 and ~1.32 kW cm^{-2} with a sampling interval of 10 ms. The average on/off times at the two excitation intensities are: ($I \approx 0.52$ kW cm^{-2}; $\langle\tau_{on}\rangle \approx 0.97$ s, $\langle\tau_{off}\rangle \approx 0.44$ s: $I \approx 1.32$ kW cm^{-2}; $\langle\tau_{on}\rangle \approx 0.32$ s, $\langle\tau_{off}\rangle \approx 0.43$ s). Intensity-dependent studies were carried out on CdSe nanocrystals with ~4 monolayers of ZnS on their surface. *b*, Fluorescence-intensity versus time trace of a 'bare' nanocrystal compared with that of an overcoated one with a shell thickness of ~7 monolayers of ZnS (ZnS 7) at the same excitation intensity ($I \approx 0.70$ kW cm^{-2}) and a sampling interval of 20 ms.

average off time yields the average neutralization time ($\langle\tau_n\rangle$) and the photoionization branching ratio, σ_I, defined as the ionization probability per excitation, is determined from the product of the excitation rate and the average on time. Consistent with photoionization/neutralization across a barrier, $\langle\tau_n\rangle$ increases and σ_I decreases with increasing shell thickness. A simple resonant tunnelling mechanism through the ZnS shell would exhibit a similar trend. Based on known band offsets between CdSe and ZnS and the electron/hole confinement energies, simple resonant tunnelling however predicts a relative branching ratio between the 'bare' and the 7-monolayer ZnS-shell sample that is two orders of

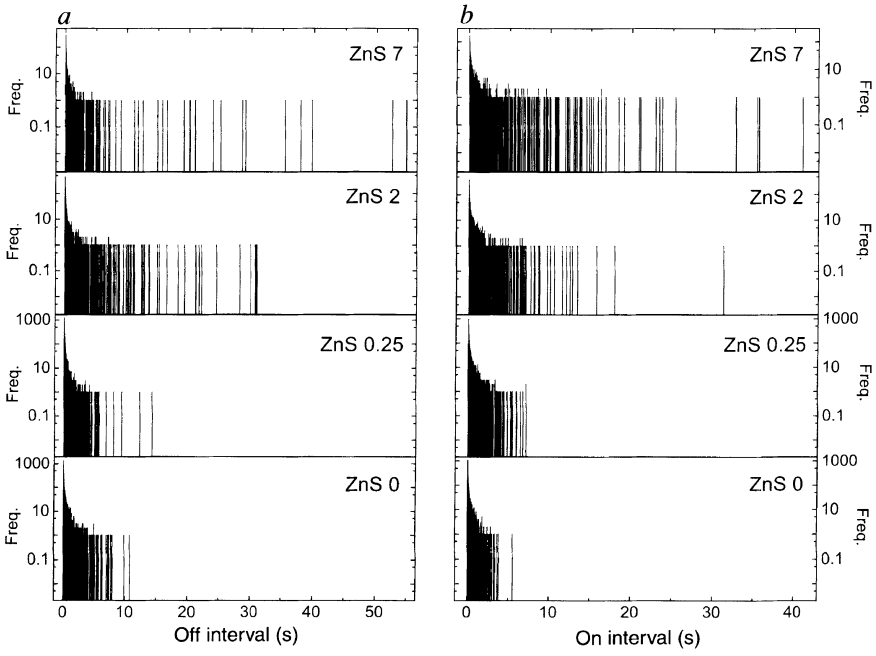

FIG. 3 *a*, Histograms of on times for CdSe nanocrystals overcoated with 0, 0.25, 2 and 7 monolayers of ZnS. The ZnS coverage was determined using quantitative X-ray spectroscopy (WDS) and small-angle X-ray scattering (SAXS). Individual histograms include statistics from 18 nanocrystals with each nanocrystal being probed for 2.73 min with a 20-ms sampling interval and an excitation intensity (I) of ~0.70 kW cm^{-2}. The average on times ($\langle\tau_{on}\rangle$) for the four samples in order of increasing shell thickness are 0.2, 0.28, 0.62 and 1.52 s with corresponding photoionization branching ratios ($\sigma_I = h\nu/\sigma I\langle\tau_{on}\rangle$) of 5.1×10^{-6}, 3.6×10^{-6}, 1.6×10^{-6} and 6.7×10^{-7} respectively. The absorption cross-section, σ, for these nanocrystals (~ 5.2×10^{-16} cm^2 at a wavelength of 532 nm) was obtained from solution measurements. *b*, Histograms of off times for the four samples from the same dataset as in *a*. The average off (neutralization) times ($\langle\tau_n\rangle$) in order of increasing shell thickness are 0.29, 0.31, 0.74 and 1.24 s.

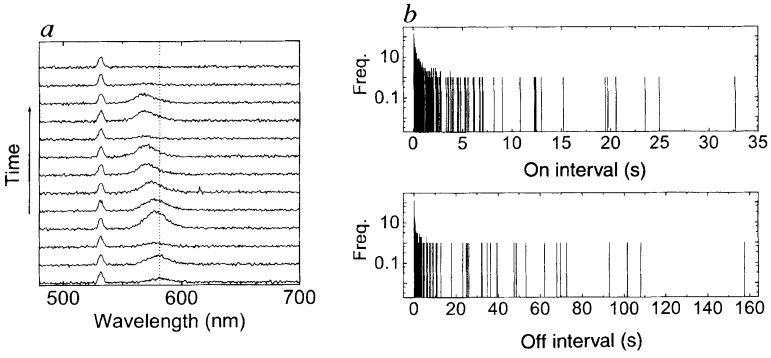

FIG. 4 *a*, Fluorescence spectra (1 min integration per spectrum) of a single nanocrystal as a function of time. The sharper feature to the blue (wavelength $\lambda = 532$ nm) is residual laser light which is included for reference. Fluctuations in fluorescence intensity relative to the laser are due to the discrete turning on and off of the emission during the experiment. Assuming an effective mass model for the quantum-confined energy levels of the nanocrystal[20], the observed blue-shift with time (~50 meV) corresponds to a ~1.75-Å shrinkage in the radius representing ~2/3 of a monolayer of CdSe. The fluorescence signal vanishes permanently in the thirteenth minute. *b*, Histograms of on/off times for a single 'robust' nanocrystal (see text) probed for ~39 min with a sampling interval of 40 ms and an excitation intensity of ~0.53 kW cm^{-2}.

magnitude larger than that observed experimentally. An 'over-the-barrier' process such as Auger ionization should be significantly less sensitive to shell thickness.

Although the nanocrystals are ionized and then neutralized reversibly, single-nanocrystal spectra shift irreversibly to the blue (Fig. 4*a*). As the quantum-confined energy levels vary as 1/radius^2, this blue-shift indicates a shrinkage of the effective radius as a function of time and is most probably due to surface photooxidation[16]. This probably causes nanocrystals to photobleach permanently before we can accumulate accurate single-dot statistics. But sometimes we find 'robust' nanocrystals which we have been able to study for up to 40 minutes under constant illumination at room temperature. In Fig. 4*b* we show the on/off histograms of one such nanocrystal. Both these distributions, which are also highly non-exponential, strongly suggest that even a single nanocrystal exhibits distributed kinetics, in sharp contrast to a single molecule which usually has a single exponential intersystem crossing rate and triplet lifetime[17,18]. A 21-Å-radius nanocrystal consists of ~1,400 atoms, of which ~25% lie on the surface. Surface reconstructions, defects and progressive oxidation could potentially lead to a range of ionization/neutralization rates.

The on/off kinetics, obscured in previous ensemble studies, reveal that although ionization is rare (probability per excitation is ~10^{-6}), it has a significant effect on luminescence count rates owing to the unusually long ($\tau_n \approx 0.5$ s) neutralization times that follow. This poses a potential limitation to optical devices based on CdSe nanocrystals for which fast response times and high luminescence efficiency are crucial. Approaches for modifying this on/off behaviour could include the use of an inorganic shell material with lattice matching superior to ZnS. Alternatively, because the on/off behaviour currently observed depends on the degree of stabilization of the ejected carrier within the matrix, this phenomenon could conceivably be exploited as a sensitive probe (especially in biological systems) of the polarity of the local environment.

Received 1 July; accepted 24 September 1996.

1. Alivisatos, A. P. *Science* **271,** 933–937 (1996).
2. Brus, L. E. *Appl. Phys. A* **53,** 465–474 (1991).
3. Colvin, V. L., Schlamp, M. C. & Alivisatos, A. P. *Nature* **370,** 354–357 (1994).
4. Dabbousi, B. O., Bawendi, M. G., Onitsuka, O. & Rubner, M. F. *Appl. Phys. Lett.* **66,** 1316–1318 (1995).
5. Weisbuch, C. *J. Cryst. Growth* **138,** 776–785 (1994).
6. Kirstaedter, N. *et al. Appl. Phys. Lett.* (in the press).
7. Schröck, E. *et al. Science* **273,** 494–497 (1996).
8. Hines, M. A. & Guyot-Sionnest, P. *J. Phys. Chem.* **100,** 468–471 (1996).
9. Kortan, A. R. *et al. J. Am. Chem. Soc.* **112,** 1327–1332 (1990).
10. Ambrose, W. P., Basche, T. & Moerner, W. E. *J. Chem. Phys.* **95,** 7150–7163 (1991).
11. Bernard, J., Fleury, L., Talon, H. & Orrit, M. *J. Chem. Phys.* **98,** 850–859 (1993).
12. Chepic, D. I. *et al. J. Lumin.* **47,** 113–127 (1990).
13. Roussignol, P., Ricard, D., Lukasik, J. & Flytzanis, C. *J. Opt. Soc. Am. B* **4,** 5–13 (1987).
14. Murray, C. B., Norris, D. J. & Bawendi, M. G. *J. Am. Chem. Soc.* **115,** 8706–8715 (1993).
15. Becerra, L. R., Murray, C. B., Griffin, R. G. & Bawendi, M. G. *J. Chem. Phys.* **100,** 3297–3300 (1994).
16. Bowen Katari, J. E., Colvin, V. L. & Alivisatos, A. P. *J. Phys. Chem.* **98,** 4109–4117 (1994).
17. Basche, T., Kummer, S. & Brauchle, C. *Nature* **373,** 132–134 (1995).
18. Cook, R. J. & Kimble, H. J. *Phys. Rev. Lett.* **54,** 1023–1026 (1985).
19. Macklin, J. J., Trautman, J. K., Harris, T. D. & Brus, L. E. *Science* **272,** 255–258 (1996).
20. Norris, D. J. & Bawendi, M. G. *Phys. Rev. B* **53,** 16338–16346 (1996).

ACKNOWLEDGEMENTS. We thank Al. L. Efros for extensive conversations.

CORRESPONDENCE should be addressed to M.N. (e-mail: nirmal@chem.columbia.edu).

Efficient real-time confocal microscopy with white light sources

R. Juškaitis, T. Wilson, M. A. A. Neil & M. Kozubek

Department of Engineering Science, University of Oxford, Parks Road, Oxford OX1 3PJ, UK

THE main advantage of confocal microscopes over their conventional counterparts arises from their ability to optically 'section' nearly transparent materials; the thin image slices thus obtained can be used to reconstruct three-dimensional images, a capability which is particularly useful for the study of biological specimens. Confocal microscopes have previously used either a single laser-illuminated point-source and single point-detector (which are scanned in tandem across the object) or white-light illumination with multiple point-sources and detectors. Single-point-source systems, however, do not usually form images in real time and are restricted to using available laser wavelengths. Multiple-point-source systems, on the other hand, produce images in real time but use light very inefficiently—typically 1% or less is used for imaging. Here we demonstrate a white-light, multiple-point-source method which can in principle produce images in real time with light efficiencies as high as 50%. This system is likely to find broad practical application, particularly in the imaging of weakly reflecting or weakly fluorescent specimens.

In order to build a confocal microscope, it is necessary to ensure that the illumination and detection systems are arranged such that light which has originated from a specific position in the source plane is detected only at the equivalent position in the detector plane[1]. This is trivial to achieve in single pinhole source/detector systems where scanning is also required to image a finite region of the object. In multiple point, tandem scanning reflection systems[2] the pinholes must be well spaced to minimize crosstalk between neighbouring 'confocal systems' and this leads to inefficient use of the available light—typically only 0.5–1.0% is used. It is also necessary to scan in order to fill in the gaps between portions of the object probed by the well spaced 'confocal systems'. Our approach is fundamentally different and does not require scanning. Let us consider the reflection system of Fig. 1. The key element is the aperture mask which consists of an array of apertures which are packed as closely together as closely together as possible in order